O(αs2)? corrections to e+e-→t t ‾ total and differential cross sections near threshold

著者	隅野　行成
journal or publication title	Physical review. D
volume	60
number	11
page range	114014-1-114014-11
year	1999
URL	http://hdl.handle.net/10097/35286

doi: 10.1103/PhysRevD.60.114014

$O(\alpha_s^2)$ corrections to $e^+e^-\to t\bar{t}$ total and differential cross sections near threshold

T. Nagano, A. Ota, and Y. Sumino
Department of Physics, Tohoku University, Sendai 980-8578, Japan
(Received 24 May 1999; published 5 November 1999)

Recently full $O(\alpha_s^2,\alpha_s\beta,\beta^2)$ corrections to the threshold total cross section for $e^+e^-\to t\bar{t}$ have been calculated, and the reported corrections turned out to be unexpectedly large. We study how to reduce the theoretical uncertainties of the cross section. We adopt a new mass definition proposed by Beneke, which incorporates a renormalon-pole cancellation in the total energy of a static quark-antiquark pair. This improves the convergence of the 1S resonance mass, while the normalization of the cross section scarcely changes. We argue that resummations of logarithms are indispensable, since two largely separated scales dictate the shape of the cross section. As a first step, we resum logarithms in the Coulombic part of the $t\bar{t}$ potential, and observe a considerable improvement in the convergence of corresponding corrections. There still remain, however, large corrections, which arise from a $1/r^2$ term in the $t\bar{t}$ potential. We also calculate full $O(\alpha_s^2,\alpha_s\beta,\beta^2)$ corrections to the momentum distributions of top quarks in the threshold region. Corrections to the distribution shape are of moderate size over the whole threshold region. [S0556-2821(99)02321-8]

PACS number(s): 14.65.Ha, 12.38.Bx, 12.38.Cy, 13.85.Lg

I. INTRODUCTION

The top quark pair production in the threshold region at future e^+e^- or $\mu^+\mu^-$ colliders is considered as an ideal process for precision measurements of top quark properties. Already many works have been devoted to the analyses of this process both theoretically and experimentally [1–29].

Recently full $O(\alpha_s^2,\alpha_s\beta,\beta^2)$ corrections to the total cross section for $e^+e^-\to\gamma^*\to t\bar{t}$ in the threshold region have been calculated independently by [23,24] using the nonrelativistic QCD (NRQCD) formalism.[1] Both calculations showed that these corrections are surprisingly large. Moreover, they found very poor convergence of the cross section as they compared the leading-order (LO), next-to-leading order (NLO) and next-to-next-to-leading order (NNLO) calculations. Theoretically, the calculation in [24] is more sophisticated in that in the vicinity of each resonance pole it includes all $O(\alpha_s^2)$ corrections to the resonance mass and to the residue. (Practically, the location of the 1S resonance peak will provide important information related to the top quark mass.) The two calculations were reproduced in [25], where some numerical error of [24] was corrected. There appeared other observations which noted potentially large theoretical uncertainties on different grounds [26,27].

In this paper, we first study how to cure the problem of the bad convergence of the total cross section observed in the above works. One possible modification is to redefine the top quark mass. It was found [30–32] that a renormalon pole contained in the QCD potential between a static quark-antiquark pair gets canceled in the total energy of the pair $2m_{\rm pole}+V_{\rm QCD}(r)$ if the pole mass $m_{\rm pole}$ is expressed in terms of the modified minimal subtraction scheme ($\overline{MS}$) mass. As a result, the series expansion of this total energy in the $\overline{MS}$ coupling $\alpha_s(\mu)$ behaves better if we use the $\overline{MS}$ mass instead of the pole mass. This suggests that the $\overline{MS}$ mass has a more natural relation to physical quantities of a static (or non-relativistic) quark-antiquark system. Beneke proposed a new quark mass definition, which incorporates a renormalon pole cancellation, and which is related to the $\overline{MS}$ mass in a well-behaved series [31].[2] We adopt this new mass definition and study the convergence properties of the $t\bar{t}$ threshold cross section.

As another improvement, we incorporate a log resummation in the cross section. There is a logical necessity for resummations of logarithms in calculations of the total cross section in the threshold region. This feature is qualitatively different from energy regions far above the threshold. In the vicinity of distinct resonance peaks (for a realistic top quark this corresponds only to the 1S peak), the total cross section takes a form

$$\sigma_{\rm tot}(s)\sim -{\rm Im}\sum_n \frac{|\psi_n(0)|^2}{\sqrt{s}-M_n+i\Gamma_n}. \tag{1}$$

The resonance spectra M_n's are dictated by the shape of the quark-antiquark QCD potential at the scale of Bohr radius $r\sim(\alpha_s m_q)^{-1}$, while the wave functions at the origin $\psi_n(0)$'s are determined by the shape of the potential at a considerably shorter distance, $1/m_q<r\ll(\alpha_s m_q)^{-1}$. Thus, in order to predict reliably both the energy dependence and normalization of the total cross section in the resonance region, one needs to calculate the shapes of the QCD potential accurately at largely separated two scales. This naturally requires log re-

[1]Corrections induced by the axial-vector coupling to a Z-exchange have been calculated, which also contribute as $O(\alpha_s^2,\alpha_s\beta,\beta^2)$ corrections [2,29].

[2]A problem is that the relation between the $\overline{MS}$ mass and the pole mass is known only up to $O(\alpha_s^2)$ [33]. Meanwhile, if we want to use the $\overline{MS}$ mass in the NNLO analyses of the threshold cross sections, we need to know this relation up to $O(\alpha_s^4)$, since the binding energies of the boundstates are $\sim\alpha_s^2 m$ already at LO.

summations using renormalization-group equations. At NLO, a log resummation was incorporated first in [3]. As a first step at NNLO, we resum logarithms in the Coulombic part of the $t\bar{t}$ potential in this work.

The second subject of this paper is a calculation of full $O(\alpha_s^2,\alpha_s\beta,\beta^2)$ corrections to the momentum distribution of top quarks in the threshold region. It is expected that the top momentum distribution will provide important information independent of those from the total cross section [5–7,15]. We therefore study how the distribution are affected by the corrections. We find that the sizes of corrections to the distribution shape are moderate in comparison with the corrections to the total cross section.

We note here that in our analyses no consistent treatment of the decay process of top quarks is attempted. Following [23,24] we merely replace the non-relativistic Hamiltonian as

$$H_{\rm NR}\to H_{\rm NR}-i\Gamma_t, \quad (\Gamma_t:\ \text{top-quark on-shell width}) \tag{2}$$

which is the correct prescription for calculating the total cross section at LO [1] and at NLO [11–15] [provided we include $O(\alpha_s)$ corrections to Γ_t [34,35] at NLO]. At NNLO, corrections related to the top decay process have not been calculated yet. As for the differential cross sections, the above prescription is valid only at LO. At NLO, the final-state interactions affect the differential cross sections non-trivially in the threshold region but cancel out in the total cross section [12,13,15,21,22]; see also [36–38].

In Sec. II we recalculate the total cross sections at LO, NLO and NNLO. Then we incorporate a new mass definition in Sec. III. We examine the effect of a log resummation in the Coulombic potential in Sec. IV. The momentum distributions of top quarks including full $O(\alpha_s^2)$ corrections are presented in Sec. V. Sec. VI contains summary and discussion. In Appendix A all notations and definitions are collected. A derivation of the momentum distribution at NNLO is presented in Appendix B, while in Appendix C we prove the unitarity relation between the total cross section and the momentum distribution.

II. TOTAL CROSS SECTION

As derived in [24], the photon-exchange contribution to the $e^+e^-\to t\bar{t}$ threshold total cross section including full $O(\alpha_s^2,\alpha_s\beta,\beta^2)$ corrections is given by

$$\sigma_{\rm tot}(s)=\frac{32\pi^2\alpha^2}{s^2}N_cQ_t^2\left\{1+\left(\frac{\alpha_s(m_t)}{\pi}\right)C_FC_1+\left(\frac{\alpha_s(m_t)}{\pi}\right)^2C_FC_2(r_0)\right\}\times{\rm Im}\left[\left(1+\frac{E+i\Gamma_t}{6m_t}\right)G(r_0,r_0)\right]. \tag{3}$$

Here, C_1 and $C_2(r_0)$ are vertex renormalization constants; their explicit forms are given in Appendix A. The Green function is defined by

$$\left\{-\frac{1}{m_t}\left[\frac{d^2}{dr^2}+\frac{2}{r}\frac{d}{dr}\right]+V(r)-\left[\omega+\frac{\omega^2}{4m_t}\right]\right\}G(r,r')=\frac{1}{4\pi rr'}\delta(r-r'), \tag{4}$$

where

$$V(r)=V_{\rm C}(r)-\frac{3\omega}{2m_t}\frac{C_F\alpha_s(\mu)}{r}-\frac{C_F(3C_A+2C_F)\alpha_s(\mu)^2}{6m_tr^2}, \tag{5}$$

$$V_{\rm C}(r)=-C_F\frac{\alpha_s(\mu)}{r}\left[1+\left(\frac{\alpha_s(\mu)}{4\pi}\right)\{2\beta_0\log(\mu'r)+a_1\}+\left(\frac{\alpha_s(\mu)}{4\pi}\right)^2\left\{\beta_0^2\left(4\log^2(\mu'r)+\frac{\pi^2}{3}\right)+2(\beta_1+2\beta_0a_1)\log(\mu'r)+a_2\right\}\right], \tag{6}$$

$$\omega=E+i\Gamma_t,\quad E=\sqrt{s}-2m_t. \tag{7}$$

In the above formulas m_t and Γ_t denote the pole mass and the decay width of top quark, respectively. $V_{\rm C}(r)$ is the Coulombic part of the $t\bar{t}$ potential $V(r)$ including the full second order corrections. Definitions of all parameters in the above formulas are collected in Appendix A.

Equation (3) includes not only all $O(\alpha_s^2,\alpha_s\beta,\beta^2)$ corrections to the LO cross section but also, in the vicinity of each resonance peak, all $O(\alpha_s^2)$ corrections to the resonance pole position and to its residue.[3] The only difference of Eq. (3) from the corresponding formula in [24] is a factor $i\Gamma_t/6m_t$, which arises from a relativistic correction to the $t\bar{t}$ kinetic energy, $\mathbf{p}^4/4m_t^3$, and from a relativistic correction to the $t\bar{t}$ production vertex, $\tilde{\psi}^\dagger\sigma^i(\overleftrightarrow{\triangle}/12m_t^2)\tilde{\chi}$. This factor is omitted incorrectly in [24]; numerically its contribution is negligible.[4]

For $\Gamma_t=0$, Eq. (3) becomes independent of the cutoff r_0 as $r_0\to 0$ up to the order of our interest. For $\Gamma_t>0$ there are uncanceled $1/r_0$ and $\log r_0$ singularities due to our improper treatment of t decay processes. Thus, following [24] we expand Eq. (3) in r_0 and omit all terms that vanish as $r_0\to 0$, and then we set

$$r_0=\frac{e^{2-\gamma_E}}{2m_t}. \tag{8}$$

[3]Hereafter we write $O(\alpha_s)$, $O(\alpha_s^2)$, etc. instead of $O(\alpha_s,\beta)$, $O(\alpha_s^2,\alpha_s\beta,\beta^2)$, etc. for the sake of simplicity.

[4]The authors of [24] claim that they incorporate the top quark width via replacement $E\to E+i\Gamma_t$. Nevertheless, they do not follow this prescription consistently in their derivation of $\sigma_{\rm tot}(s)$ and overlook the factor $i\Gamma_t/6m_t$.

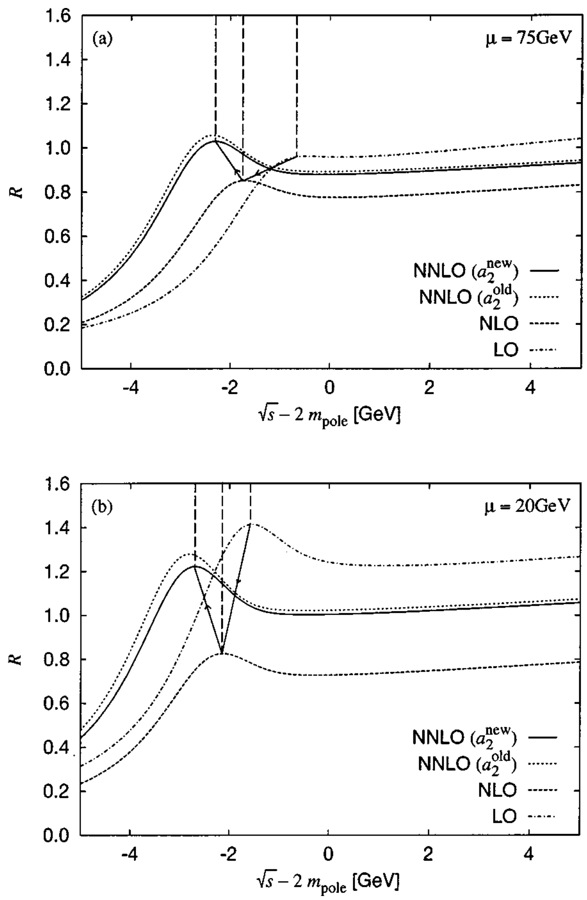

FIG. 1. R-ratios for $e^+e^-\to t\bar{t}$ at LO (dot-dashed), NLO (dashed), and NNLO (solid) as functions of the energy measured from twice the pole mass, $\sqrt{s}-2m_{\rm pole}$. Arrows indicate dislocations of the maximum point of R as the $O(\alpha_s)$ and $O(\alpha_s^2)$ corrections are included, respectively. We set $m_{\rm pole}=m_t=175$ GeV, $\Gamma_t=1.43$ GeV, and $\alpha_s(m_Z)=0.118$. Dotted lines show NNLO R-ratios calculated with an old value of a_2 [42], which is one of the coefficients in the two-loop perturbative QCD potential. (a) is for $\mu=75$ GeV and (b) is for $\mu=20$ GeV.

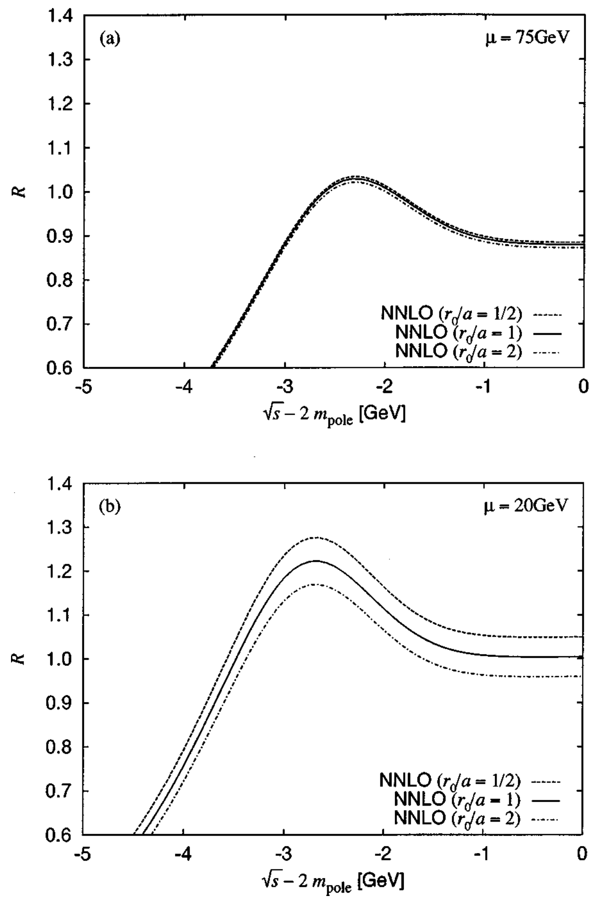

FIG. 2. R-ratios for $e^+e^-\to t\bar{t}$ at NNLO for several values of r_0: $r_0 = a/2$ (dashed), $r_0=a$ (solid), and $r_0=2a$ (dot-dashed), where $a\equiv e^{2-\gamma_E}/2m_t$. (a) is for $\mu=75$ GeV, and (b) is for $\mu=20$ GeV. Other notations and parameters are same as in Fig. 1.

We also set $m_t=175$ GeV, $\Gamma_t=1.43$ GeV and $\alpha_s(m_Z)=0.118$ in our numerical analyses below. As a cross check of our calculations, we reproduced the total cross sections calculated in [25].

In Figs. 1 we compare the R-ratio $R(s)=\sigma_{\rm tot}/\sigma_{\rm pt}$ at LO, NLO, and NNLO ($\sigma_{\rm pt}=4\pi\alpha^2/3s$). As noted in [23,24] the cross section changes considerably as we include $O(\alpha_s)$ and $O(\alpha_s^2)$ corrections, respectively. One sees that, as we include these corrections, convergence of the normalization of the cross section is better for $\mu=75$ GeV than that for $\mu=20$ GeV, whereas convergence of the peak position ($\simeq$ mass of the $1S$ resonance) is better for $\mu=20$ GeV than that for $\mu=75$ GeV. This indicates that the peak position is determined mainly by the shape of the potential $V(r)$ at the Bohr scale $\sim(\alpha_s m_t)^{-1}$, while the normalization of the cross section is determined by the shape of $V(r)$ at a shorter distance; note that corrections to the potential are minimized around $r\simeq 1/\mu' = e^{-\gamma_E}/\mu$. In the same figure we also show the cross section calculated using an old value [42] of a_2 in $V_{\rm C}(r)$, which has been corrected recently [43]. A change of the cross section caused by correcting a_2 is small.

In Figs. 2 we vary the value of r_0 by factors 2 and 1/2. The cross section varies correspondingly, which is generated by $O(\alpha_s^3)$ and $O(\Gamma_t/m_t)$ terms in Eq. (3). The sizes of the variations serve as a measure of uncertainties of our theoretical prediction. They seem to be rather small as compared to what one naively expects from the poor convergence properties seen in Figs. 1.

III. REDEFINITION OF TOP QUARK MASS

According to Beneke [31], we define a new quark mass appropriate in the threshold region (the potential-subtracted mass) by adding an infra-red portion of the Coulombic potential to the pole mass. In this way the new mass is related to the $\overline{MS}$ mass in a more convergent series than to the pole mass (in our case $m_{\rm pole}=m_t$):

$$m_{\rm PS}(\mu_f)\equiv m_{\rm pole}+\Delta m(\mu_f), \tag{9}$$

$$\Delta m(\mu_f)\equiv\frac{1}{2}\int_{|\mathbf{q}|<\mu_f}\frac{d^3\mathbf{q}}{(2\pi)^3}\tilde{V}_{\rm C}(q), \tag{10}$$

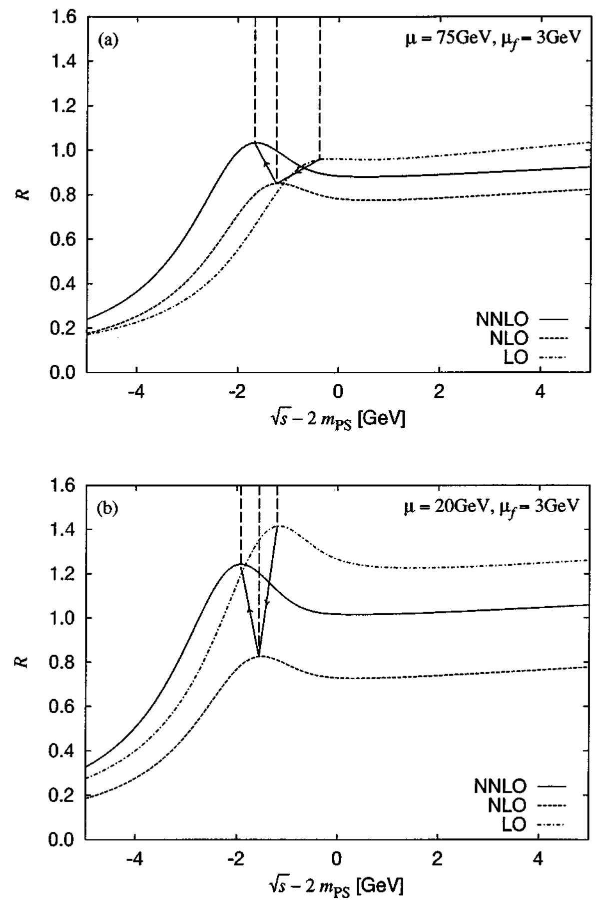

FIG. 3. R-ratios for $e^+e^- \to t\bar{t}$ at LO (dot-dashed), NLO (dashed), and NNLO (solid) as functions of the energy measured from twice the potential-subtracted mass, $\sqrt{s} - 2m_{\mathrm{PS}}$. We set $\mu_f = 3$ GeV and $m_{\mathrm{PS}}(\mu_f) = 175$ GeV. (a) is for $\mu = 75$ GeV, and (b) is for $\mu = 20$ GeV. Other notations and parameters are same as in Fig. 1.

where $\tilde{V}_{\mathrm{C}}(q)$ is the Fourier transform of the Coulombic potential $V_{\mathrm{C}}(r)$.[5] At the same time we subtract a corresponding part from the potential as

$$V_{\mathrm{C}}(r;\mu_f) \equiv V_{\mathrm{C}}(r) - 2\Delta m(\mu_f) \tag{11}$$

such that the total energy of a quark-antiquark pair remains unchanged in both schemes:

$$2m_{\mathrm{pole}} + V_{\mathrm{C}}(r) = 2m_{\mathrm{PS}}(\mu_f) + V_{\mathrm{C}}(r;\mu_f). \tag{12}$$

In Fig. 3 are shown the LO, NLO and NNLO total cross section by fixing $m_{\mathrm{PS}}(3\ \mathrm{GeV}) = 175$ GeV. It can be seen that the convergence of the $1S$ peak position becomes better as expected. Meanwhile the normalization of the cross section scarcely changes by this modification. It is because Eq. (9) essentially incorporates a constant shift of the cross section in the horizontal direction by an amount $\Delta m(\mu_f)$, while changes in the normalization generated by a modification of the mass in the Schrödinger equation (4) is negligibly small.

IV. RENORMALIZATION-GROUP IMPROVEMENT OF $V_{\mathrm{C}}(R)$

As already mentioned, it is important to resum logarithms in calculations of threshold cross sections. We demonstrate[6] an improvement of convergence of the cross section by incorporating log resummations to the Coulombic potential $V_{\mathrm{C}}(r)$.

The Coulombic potential $V_{\mathrm{C}}(r)$ is identified with the QCD potential between a static quark-antiquark pair. If we write this potential in momentum space [Fourier transform of Eq. (7)] as

$$\tilde{V}_{\mathrm{C}}(q) = -4\pi C_F \frac{\alpha_V(q;\mu)}{q^2}, \tag{13}$$

a log resummation using a renormalization group equation is achieved simply by a replacement $\mu \to q$ [42]:

$$\tilde{V}_{\mathrm{C}}^{(RG)}(q) = -4\pi C_F \frac{\alpha_V(q;q)}{q^2}. \tag{14}$$

Hence, in accordance with the formulation in the previous section, we define a potential-subtracted mass and a renormalization-group-improved potential in coordinate space, respectively, as

$$m_{\mathrm{PS}}(\mu_f) \equiv m_{\mathrm{pole}} + \Delta m(\mu_f),$$

$$\Delta m(\mu_f) \equiv \frac{1}{2}\int_{|\mathbf{q}|<\mu_f} \frac{d^3\mathbf{q}}{(2\pi)^3} \tilde{V}_{\mathrm{C}}^{(RG)}(q), \tag{15}$$

$$\begin{aligned} V_{\mathrm{C}}^{(RG)}(r;\mu_f) &\equiv \int_{|\mathbf{q}|>\mu_f} \frac{d^3\mathbf{q}}{(2\pi)^3} e^{i\mathbf{q}\cdot\mathbf{r}} \tilde{V}_{\mathrm{C}}^{(RG)}(q) \\ &= V_{\mathrm{C}}^{(RG)}(r;\mu_f=0) \\ &\quad - \int_{|\mathbf{q}|<\mu_f} \frac{d^3\mathbf{q}}{(2\pi)^3} e^{i\mathbf{q}\cdot\mathbf{r}} \tilde{V}_{\mathrm{C}}^{(RG)}(q). \end{aligned} \tag{16}$$

In this formulation both m_{pole} and $\Delta m(\mu_f)$ suffer from theoretical uncertainties of the order $\sim \Lambda_{\mathrm{QCD}}$ due to the renormalon poles, but they cancel in $m_{\mathrm{PS}}(\mu_f)$. We note that strictly speaking there is no guiding principle for subtracting also a r-dependent part from the potential in (16), since there is no known renormalon cancelation related to r-dependent part of the potential. In fact the total energy of a quark-antiquark pair (12) is not well-defined after the renormalization-group improvement (14), and a theoretical

[5]Note that our $\Delta m(\mu_f)$ is related to a corresponding quantity in [31] by $\Delta m(\mu_f) = -\delta m(\mu_f)$.

[6]A full resummation of logarithms up to NNLO requires a significant modification of the formulas (3) and (4); we will study its incorporation in our future work.

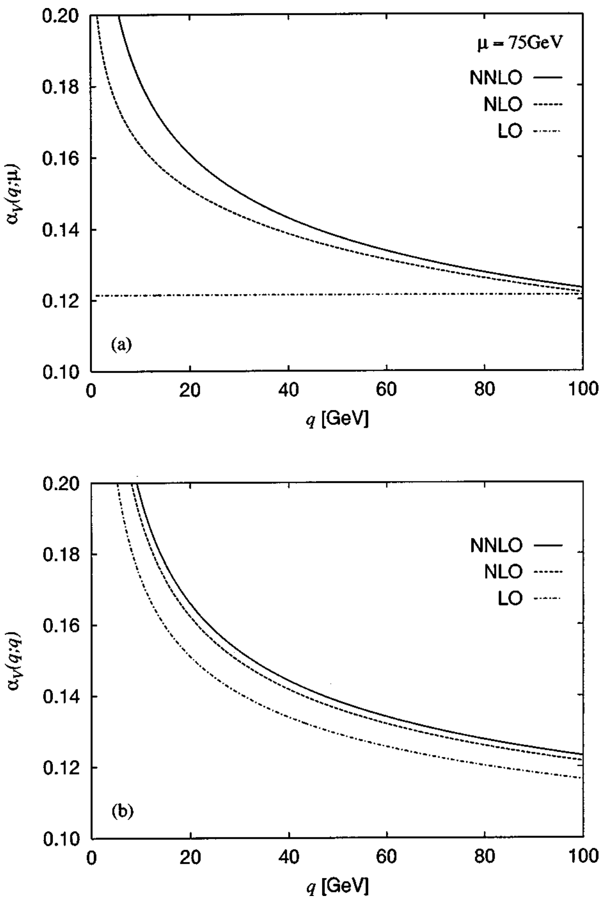

FIG. 4. The momentum-space couplings α_V vs momentum transfer q at LO (dot-dashed), NLO (dashed), and NNLO (solid). (a) is the fixed-order coupling ($\mu = 75$ GeV), and (b) is a renormalization-group improved coupling ($\mu = q$).

ambiguity of the order $\sim \Lambda_{\rm QCD}^2 r$ is caused by a non-canceled renormalon pole in the r-dependent part.[7] This ambiguity is negligible in our case thanks to the large mass and decay width of the top quark [1]; see [3–5] for more practical analyses. Thus, we should set $\mu_f \gg \Lambda_{\rm QCD}$ in order to avoid a bad convergence of the cross section generated by a renormalon pole, while we should set $\mu_f \ll \alpha_s m_t$ such that a main part of bound-state dynamics is preserved. In our analyses below we choose $\mu_f = 3$ GeV. [We have checked that upon varying μ_f the cross section changes only by a constant shift in the horizontal direction and a change in the normalization is negligible, i.e. r-dependence of the subtracted part in (16) plays no significant role.][8]

We compare the couplings of the momentum-space potential with $[\alpha_V(q;q)]$ and without $[\alpha_V(q;\mu = 75 \text{ GeV})]$ a renormalization-group improvement in Figs. 4. One sees that convergence of the coupling improves drastically by the log resummation over the whole range of our interest, $m_t^{-1} < r \lesssim (\alpha_s m_t)^{-1}$. One therefore anticipates that $O(\alpha_s)$ and $O(\alpha_s^2)$ corrections to the total cross section originating from $V_{\rm C}(r)$ also become smaller and more converging. In order to see only these corrections separately, we show in Fig. 5 the R-ratio calculated from

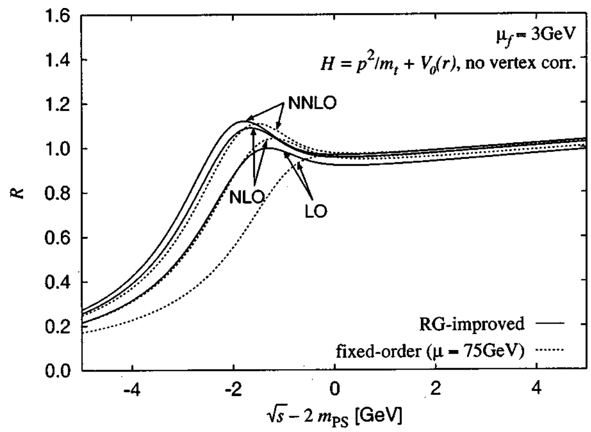

FIG. 5. R-ratios for $e^+e^- \to t\bar{t}$ calculated with a Hamiltonian $H = p^2/m_t + V_0(r)$, where $V_0(r)$ includes only the Coulombic part of the $t\bar{t}$ potential. Other corrections (vertex renormalization constants, kinematical corrections, etc.) are not included. Solid and dashed lines, respectively, show R-ratios with $[V_0(r) = V_{\rm C}^{(RG)}(r;\mu_f)]$ and without $[V_0(r) = V_{\rm C}(r),\ \mu = 75\ \text{GeV}]$ a renormalization-group improvement of the Coulombic potential. We set $\mu_f = 3$ GeV, $m_{\rm PS}(\mu_f) = 175$ GeV, $\Gamma_t = 1.43$ GeV, and $\alpha_s(m_Z) = 0.118$.

$$R(s) = \frac{6\pi N_c Q_t^2}{m_t^2} \, \mathrm{Im}\, G(0,0) \tag{17}$$

with

$$\left\{ -\frac{1}{m_t}\left[\frac{d^2}{dr^2} + \frac{2}{r}\frac{d}{dr}\right] + V_0(r) - \omega \right\} G(r,r') = \frac{1}{4\pi r r'}\,\delta(r - r'), \tag{18}$$

both for $V_0(r) = V_{\rm C}(r)$ and $V_0(r) = V_{\rm C}^{(RG)}(r;\mu_f)$. Namely, we omit all $O(\alpha_s)$ and $O(\alpha_s^2)$ corrections other than those in the Coulombic potential. One sees clearly that the convergence property has improved considerably by the log resummations.

Finally we combine the above corrections with all other corrections. Namely we show in Fig. 6 the total cross section (3) with and without the renormalization-group improvement of the Coulombic potential. Also we list the "binding energies" of the $1S$ resonance state $2m_{\rm PS}(\mu_f) - M_{1S}$ in Table I. Although it is seen that convergence of the normalization of the cross section as well as convergence of the $1S$ resonance mass become slightly better, improvements are not so dramatic. This is because other corrections, in particular those

---

[7] Within our perturbative formalism $\sim \Lambda_{\rm QCD}^2 r$ term in the potential is forbidden by the rotational invariance, and the first ambiguous r-dependence arises at $\sim \Lambda_{\rm QCD}^3 r^2$.

[8] In rewriting the pole mass m_t in terms of $m_{\rm PS}(\mu_f)$ in Eqs. (3)-(7), we retained terms up to (and including) $O(\alpha_s^3)$ in this relation.

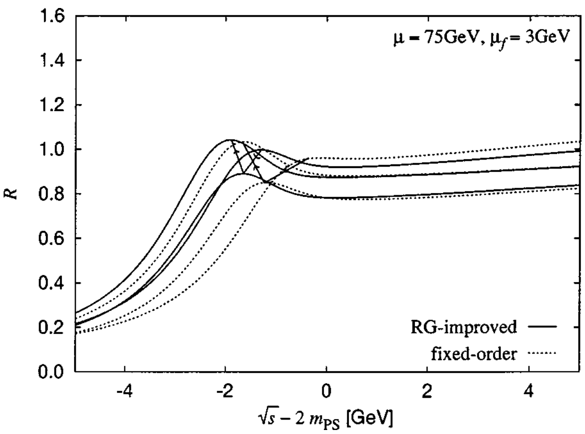

FIG. 6. R-ratios for $e^+e^-\to t\bar{t}$ at LO, NLO, and NNLO. Solid lines show those with renormalization-group improved Coulombic potentials, $V_C^{(RG)}(r;\mu_f)$. Dashed lines are those with fixed-order Coulombic potentials $V_C(r)$. Arrows indicate dislocations of the maximum point of R as the $O(\alpha_s)$ and $O(\alpha_s^2)$ corrections are included, respectively. We set $\mu_f=3$ GeV, $m_{\rm PS}(\mu_f)=175$ GeV, $\mu=75$ GeV, $\Gamma_t=1.43$ GeV, and $\alpha_s(m_Z)=0.118$.

originating from the $1/r^2$ potential in $V(r)$, are uncomfortably large. It remains as our future task to gain better understandings of these residual large corrections.

V. TOP QUARK MOMENTUM DISTRIBUTION

Using the NRQCD formalism and also techniques developed in [24], one obtains the momentum distribution of top quarks in the threshold region including all $O(\alpha_s^2)$ corrections as

$$\frac{d\sigma}{dp}=\frac{16\alpha^2}{s^2}N_cQ_q^2\left\{1+\left(\frac{\alpha_s(m_t)}{\pi}\right)C_FC_1+\left(\frac{\alpha_s(m_t)}{\pi}\right)^2C_FC_2(r_0)\right\}\times p^2\Gamma_t\, f(p;r_0), \quad (19)$$

where

$$f(p;r_0)=\left\{\left(1+\frac{2E}{3m_t}\right)|\tilde{G}(p;r_0)|^2+\frac{3}{2}C_F\alpha_s(\mu)^2\,\mathrm{Re}[\tilde{G}_{1/r}(p;r_0)\,\tilde{G}(p;r_0)^*]-\frac{11}{6}C_F\alpha_s(\mu)^2\,\mathrm{Re}[\tilde{G}_{ip_r}(p;r_0)\,\tilde{G}(p;r_0)^*]+\frac{1}{6m_t}\frac{\sin(pr_0)}{pr_0}\mathrm{Re}[\tilde{G}(p;r_0)]\right\}. \quad (20)$$

In these formulas, p denotes the magnitude of the top quark three-momentum. Momentum-space Green functions are defined from the coordinate-space Green function in (4) by

$$\tilde{G}(p;r_0)=\int d^3\mathbf{r}\,e^{i\mathbf{p}\cdot\mathbf{r}}\,G(r,r_0), \quad (21)$$

$$\tilde{G}_{1/r}(p;r_0)=\int d^3\mathbf{r}\,e^{i\mathbf{p}\cdot\mathbf{r}}\frac{1}{\alpha_s(\mu)m_tr}G(r,r_0), \quad (22)$$

$$\tilde{G}_{ip_r}(p;r_0)=\int d^3\mathbf{r}\,e^{i\mathbf{p}\cdot\mathbf{r}}\frac{ip_r}{\alpha_s(\mu)m_t}G(r,r_0), \quad (23)$$

with $ip_r=d/dr+1/r$. A derivation of the formulas is given in Appendix B. One can show that upon integrating over $\int dp$ the total cross section formula (3) is recovered. A proof of the unitarity relation between the total cross section (3) and the momentum distribution (19) is given in Appendix C. We also checked numerically that the unitarity relation holds well within our desired accuracies.

For consistency with our analyses of the total cross section, we expand Eq. (19) in terms of the cutoff r_0, omit terms regular as $r_0\to 0$, and set its value as in Eq. (8).[9] In all

TABLE I. ''Binding energies'' of the $1S$ resonance state defined as $2m_{\rm PS}(\mu_f)-M_{1S}$ at LO, NLO, and NNLO calculated with $V_C(r)$ (fixed-order) and with $V_C^{(RG)}(r;\mu_f)$ (RG-improved). We set $\mu_f=3$ GeV, $m_{\rm PS}(\mu_f)=175$ GeV, $\Gamma_t=1.43$ GeV, and $\alpha_s(m_Z)=0.118$.

	(Fixed-order)		(RG-improved)	
	$\mu=20$ GeV	$\mu=75$ GeV	$\mu=20$ GeV	$\mu=75$ GeV
LO	1.390 GeV	0.838 GeV	1.573 GeV	1.573 GeV
NLO	1.716 GeV	1.453 GeV	1.861 GeV	1.861 GeV
NNLO	2.062 GeV	1.817 GeV	2.136 GeV	2.058 GeV

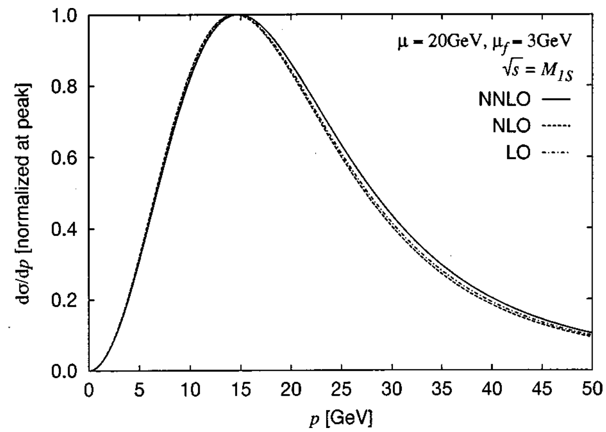

FIG. 7. Top quark momentum distributions at LO (dot-dashed), NLO (dashed), and NNLO (solid) for $\mu=20$ GeV. For each curve, we set the c.m. energy on the $1S$ resonance state, $\sqrt{s}=M_{1S}$.

[9]Note that strictly speaking the unitarity relation is violated after this expansion, because $\int dp$ integration and expansion in r_0 do not commute for $\Gamma_t>0$. Practically the unitarity relation holds to a sufficient accuracy by cuting off the momentum integration at some appropriately large scale.

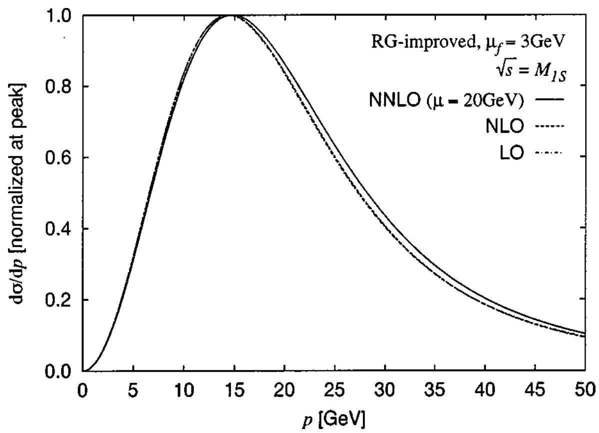

FIG. 8. Same as Fig. 7 but with a renormalization group improvement in the Coulomb part of the potential: LO (dot-dashed), NLO (dashed), and NNLO (solid).

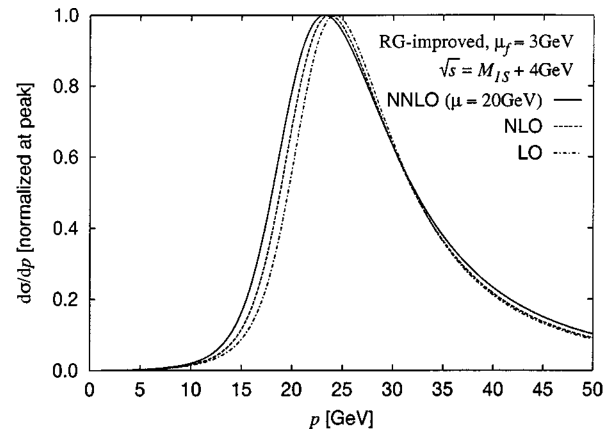

FIG. 10. Same as Fig. 9 but with a renormalization group improvement in the Coulomb part of the potential: LO (dot-dashed), NLO (dashed), and NNLO (solid).

figures we choose $\mu=20$ GeV since a relevant scale around the distribution peak is the scale of Bohr radius $\sim(\alpha_s m_t)^{-1}$.

Top quark momentum distributions (normalized to unity at each distribution peak) are shown in Figs. 7–10. Following a strategy advocated in [15], we fix the c.m. energy relative to the $1S$ resonance mass $\Delta E=\sqrt{s}-M_{1S}$ upon comparing LO, NLO and NNLO distributions. On the $1S$ resonance ($\Delta E=0$, Fig. 7), $O(\alpha_s)$ and $O(\alpha_s^2)$ corrections shift the distribution peak, $p_{\rm peak}$, by -0.8% and by $+2.5\%$, respectively. Also one sees that the $O(\alpha_s^2)$ corrections are larger at higher momentum region. This is expected because part of the $O(\alpha_s^2)$ corrections are relativistic corrections which are enhanced in the relativistic regime. In Fig. 8 we incorporate a log resummation in the Coulombic potential, i.e. replace $V_{\rm C}(r)\to V_{\rm C}^{(RG)}(r;\mu_f)$. Qualitative tendencies of the corrections are not changed by the resummation. [$\delta p_{\rm peak}/p_{\rm peak}= +0.5\%$ and $+2.2\%$ at $O(\alpha_s)$ and $O(\alpha_s^2)$, respectively.] We show momentum distributions at $\Delta E=4$ GeV in Fig. 9 [with $V_{\rm C}(r)$] and in Fig. 10 [with $V_{\rm C}^{(RG)}(r;\mu_f)$]. One sees that in both figures $O(\alpha_s)$ and $O(\alpha_s^2)$ corrections, respectively, reduce the peak momentum $p_{\rm peak}$.

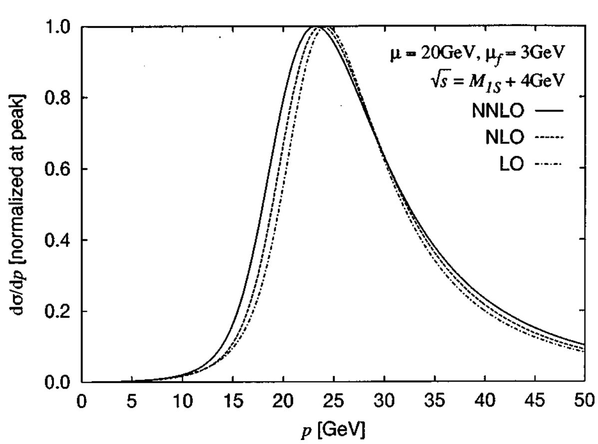

FIG. 9. Top quark momentum distributions at LO (dot-dashed), NLO (dashed), and NNLO (solid) for $\mu=20$ GeV. For each curve, we set the c.m. energy at 4 GeV above the $1S$ resonance mass.

In general, we see following energy dependences of the $O(\alpha_s)$ and $O(\alpha_s^2)$ corrections to the peak momentum $\delta p_{\rm peak}/p_{\rm peak}$. At $\Delta E=0$ the corrections are positive $\sim+$ few %; between $\Delta E=0$ and $\Delta E=1$-2 GeV, the corrections decrease and change sign from +few % to − few %; at higher energies, $\Delta E>1$-2 GeV, the corrections stay negative, but their magnitude $|\delta p_{\rm peak}/p_{\rm peak}|$ decrease with energy. The energy dependences of the $O(\alpha_s)$ and the $O(\alpha_s^2)$ corrections are qualitatively similar.

These energy dependences can be understood as a consequence of an increase of attractive force between t and $\bar{t}$.[10] Namely, at $\Delta E=0$, $p_{\rm peak}$ is determined by the binding energy and is larger for a larger binding energy. At higher energies, $\Delta E>1$-2 GeV, the peak momentum of the distribution tends to be determined only from kinematics, $p_{\rm peak} \approx\frac{1}{2}\sqrt{s-4m_t^2}$. Meanwhile, if the binding energy becomes larger due to an increase of attractive force, the $1S$ resonance mass will be lowered, and therefore $\sqrt{s}$ becomes smaller for a fixed ΔE.

In all the above results, the decay process of top quarks have been treated only effectively by the replacement (2), and we have not included in our analyses even the already known $O(\alpha_s)$ corrections which arise in relation to the top quark decay process, namely the final-state interactions between t and $\bar{t}$ decay products. For comparison, we show in Figs. 11 and 12 these effects of the $O(\alpha_s)$ final-state interactions on the top quark momentum distribution. As noted in [12,13,15,21,22], the final-state interactions reduce the peak momentum about 5% almost independently of the energy. These energy dependences are distinctly different from those of the NLO and NNLO corrections studied above. Thus, the

[10] In fact the strength of the Coulombic force, $|dV_{\rm C}/dr|$ or $|dV_{\rm C}^{(RG)}/dr|$, increases by the $O(\alpha_s)$ and $O(\alpha_s^2)$ corrections at relevant distances. (This may be seen from increases of the couplings in Fig. 4.) Also, there is an additional attractive force [$1/r^2$ term in $V(r)$] at NNLO. Thus, reflecting the increase of binding energies, the mass of the $1S$ resonance state decreases; see Table I.

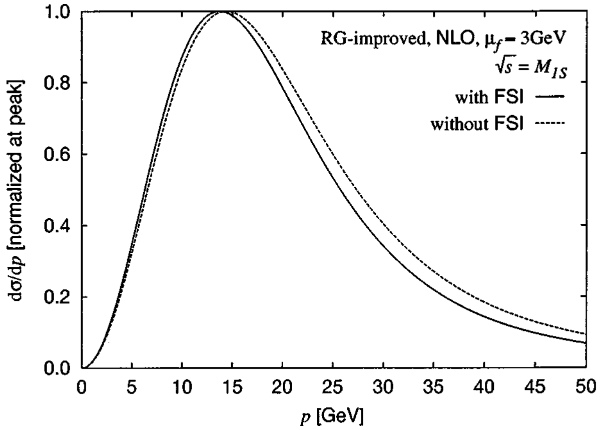

FIG. 11. Top quark momentum distributions at NLO with the renormalization group improvement for the Coulomb part of the potential. The c.m. energy is set on the $1S$ resonance state. The solid (dashed) line is calculated with (without) the $O(\alpha_s)$ final-state interaction corrections.

effects of the $O(\alpha_s)$ final-state interactions are larger and qualitatively different, so that they would be distinguishable from other NLO and NNLO corrections considered in this paper.

VI. SUMMARY AND DISCUSSION

We studied convergence properties of the total cross section for $e^+e^-\to t\bar{t}$ in the threshold region. By expressing the cross section in terms of the potential-subtracted mass $m_{\mathrm{PS}}(\mu_f)$ instead of the pole mass, a better convergence of the $1S$ resonance mass was obtained, whereas the normalization of the cross section hardly changed. We argue that log resummations are indispensable for analyses of the cross section in the threshold region. As a first step, we resummed logarithms in the Coulombic part of the $t\bar{t}$ potential by renormalization-group improvement. In this prescription, we followed closely a formulation of the potential subtraction in the fixed-order analysis. Corrections originating from the Coulombic potential became much more converging after the log resummations, both for the $1S$ resonance mass and for

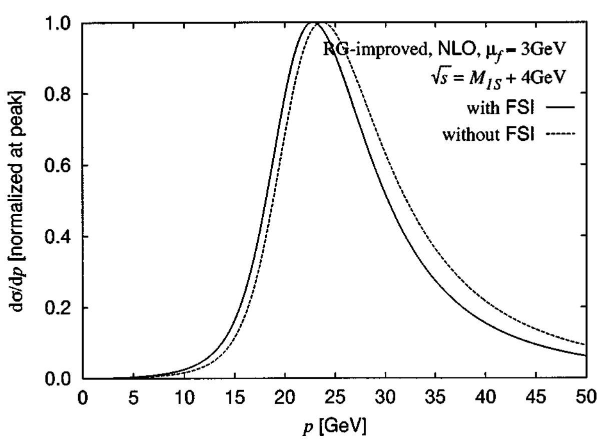

FIG. 12. Same as Fig. 11 but for the c.m. energy 4 GeV above the $1S$ resonance state.

the normalization of the cross section. There still remain, however, unexpectedly large $O(\alpha_s^2)$ corrections, whose main part arises from the $1/r^2$ term in the $t\bar{t}$ potential $V(r)$. We should implement full log resummations to the threshold cross section and see whether these large corrections remain.

We also calculated the momentum distributions of top quarks in the threshold region including full $O(\alpha_s^2)$ corrections. On the $1S$ resonance state, the $O(\alpha_s^2)$ corrections to the distribution shape are small. In particular the shift of p_{peak} is $+2.2\%$ after a renormalization-group improvement of the Coulombic potential, which seems to be of a legitimate size. At higher energies, the corrections change sign and become negative. Over the whole threshold region the size of the corrections $\delta p_{\mathrm{peak}}/p_{\mathrm{peak}}$ stays within a few percent. These features can be understood as a combined effect of kinematics and an increase of binding energy. Thus, a major part of the corrections can be traced back again to the $1/r^2$ term in $V(r)$ which affects the binding energy significantly. In addition to the full resummations of logarithms, it is mandatory to incorporate the decay process of top quarks properly in order to attain a more reliable theoretical prediction of the momentum distributions, since off-shell contributions, i.e. $\sim(p-p_{\text{on-shell}})^2/m_t^2$ corrections, are not treated correctly in the present calculation. We demonstrated that the $O(\alpha_s)$ final-state interaction corrections to the distribution shape are significant in comparison to other NLO corrections. Thus, we think that yet uncalculated $O(\alpha_s^2)$ final-state interactions may give rise to corrections which are non-negligible compared to the NNLO corrections calculated in this paper.

It was argued in [26] that a large theoretical uncertainty exists even after a renormalization-group improvement of the Coulombic potential. This claim was based on a large discrepancy between results of renormalization-group improvements in momentum space and in coordinate space. Now we have a better guiding principle. The large discrepancy originated from a renormalon pole [39,31], and by adopting an appropriate mass definition we can cancel this pole (at least in the r-independent part of the Coulombic potential) and obtain a more convergent perturbative series consequently. In this work, we adopted the potential-subtracted mass.

After completion of this work, we received a paper by Beneke, Signer, and Smirnov [28]. Their work has a significant overlap with Sec. III of the present paper. Effects of introducing $m_{\mathrm{PS}}(\mu_f)$ on the cross section are consistent between their results and ours. We adopt a value of μ_f considerably smaller than that adopted in their paper. This is in view of our application of the formalism to the renormalization-group improved potential; see discussion below Eq. (16).

ACKNOWLEDGMENTS

The authors are grateful to T. Teubner for bringing our attention to [43]. One of the authors (Y.S.) would like to thank K. Fujii, K. Melnikov, A. H. Hoang and T. Teubner for useful discussions. This work is supported by the Japanese-German Cooperative Science Promotion Program.

APPENDIX A: DEFINITIONS AND CONVENTIONS

In Eq. (3), the vertex renormalization constants are given by [23,24]

$$C_1 = -4, \quad C_2 = C_F C_2^A + C_A C_2^{NA} + T_R N_L C_2^L + T_R N_H C_2^H, \tag{A1}$$

where

$$C_2^A = \frac{39}{4} - \zeta_3 + \pi^2 \left\{ \frac{2}{3} \log(2e^{\gamma_E - 2} m_t r_0) + \frac{4}{3}\log 2 - \frac{35}{18} \right\}, \tag{A2}$$

$$C_2^{NA} = -\frac{151}{36} - \frac{13}{2}\zeta_3 + \pi^2 \left\{ \log(2e^{\gamma_E - 2} m_t r_0) - \frac{8}{3}\log 2 + \frac{179}{72} \right\}, \tag{A3}$$

$$C_2^L = \frac{11}{9}, \tag{A4}$$

$$C_2^H = \frac{44}{9} - \frac{4}{9}\pi^2. \tag{A5}$$

QCD color factors are defined as $N_c = 3$, $C_F = 4/3$, $C_A = 3$, $T_R = 1/2$, and the fermion numbers in our problem are given by $N_L = 5$ and $N_H = 1$. Also, the top quark charge is defined by $Q_t = 2/3$.

The Coulombic potential (6) is identified with the QCD potential between a static quark-antiquark pair. The first-order correction to the QCD potential was calculated in [40,41], while the second-order correction was calculated first in [42], a part of which has been corrected recently in [43]. Their coefficients are given, respectively, by

$$\beta_0 = \frac{11}{3} C_A - \frac{4}{3} T_R N_L, \tag{A6}$$

$$\beta_1 = \frac{34}{3} C_A^2 - \frac{20}{3} C_A T_R N_L - 4 C_F T_R N_L, \tag{A7}$$

$$a_1 = \frac{31}{9} C_A - \frac{20}{9} T_R N_L, \tag{A8}$$

$$a_2 = \left(\frac{4343}{162} + 4\pi^2 - \frac{\pi^4}{4} + \frac{22}{3}\zeta_3 \right) C_A^2 - \left(\frac{1798}{81} + \frac{56}{3}\zeta_3 \right) C_A T_R N_L - \left(\frac{55}{3} - 16\zeta_3 \right) C_F T_R N_L + \frac{400}{81} T_R^2 N_L^2. \tag{A9}$$

In Eq. (6), $\mu' = \mu e^{\gamma_E}$, where $\gamma_E = 0.5772\ldots$ denotes the Euler constant.

APPENDIX B: DERIVATION OF TOP QUARK MOMENTUM DISTRIBUTION

According to the NRQCD formalism, the NNLO $\gamma t\bar{t}$ vertex in the threshold region is given by

$$\Gamma^i(p,E) = \gamma^i \times \left[C(r_0) + \frac{\Delta_{r_0}}{6 m_t^2 c^2} \right] \times \left(\frac{\mathbf{p}^2}{m_t} - \frac{\mathbf{p}^4}{4 m_t^3 c^2} - \omega \right) \tilde{G}_{\rm NR}(p; r_0), \tag{B1}$$

$$\omega = E + i\Gamma_t, \quad E = \sqrt{s} - 2 m_t c^2. \tag{B2}$$

The NRQCD Green function is defined by

$$[H_{\rm NR} - \omega]\, G_{\rm NR}(\mathbf{r}, \mathbf{r}') = \delta(\mathbf{r} - \mathbf{r}'), \tag{B3}$$

$$H_{\rm NR} = \frac{\mathbf{p}^2}{m_t} - \frac{\mathbf{p}^4}{4 m_t^3 c^2} + V_{\rm C}(r) + \frac{11\pi C_F a_s}{3 m_t^2 c^2}\, \delta(\mathbf{r}) - \frac{C_F a_s}{2 m_t^2 c^2} \left\{ \frac{1}{r}, \mathbf{p}^2 \right\} - \frac{C_F C_A a_s^2}{2 m_t c^2 r^2}, \tag{B4}$$

$$\tilde{G}(p; r_0) = \int d^3\mathbf{r}\, e^{i\mathbf{p}\cdot\mathbf{r}}\, G_{\rm NR}(r, r_0), \tag{B5}$$

where $G_{\rm NR}(r,r')$ denotes the S-wave component of $G_{\rm NR}(\mathbf{r},\mathbf{r}')$. In these formulas we restored the speed of light, c, and defined $a_s \equiv \alpha_s(\mu)\, c$. Then one can identify the NLO and NNLO corrections with the coefficients of $1/c$ and $1/c^2$, respectively, in the series expansion of $\Gamma^i(p,E)$ in $1/c$ [44]. The vertex renormalization constant $C(r_0)$ is determined by matching (B1) to the 2-loop $\gamma t\bar{t}$ on-shell vertex [45].

From the relation [24]

$$H_{\rm NR} = \frac{\mathbf{p}^2}{m_t} + V_{\rm C}(r) - \frac{H_0^2}{4 m_t c^2} - \frac{3 C_F a_s}{4 m_t c^2} \left\{ H_0, \frac{1}{r} \right\} + \frac{11 C_F a_s}{12 m_t c^2} [H_0, i p_r] - \frac{C_F (3C_A + 2C_F) a_s^2}{6 m_t c^2 r^2}, \tag{B6}$$

$$H_0 = \frac{\mathbf{p}^2}{m_t} - C_F \frac{a_s}{r}, \tag{B7}$$

one may find an approximate expression for the Green function

$$G_{\rm NR}(r,r') \simeq \left[1 + \frac{\omega}{2 m_t c^2} + \frac{3 C_F a_s}{4 m_t c^2} \left(\frac{1}{r} + \frac{1}{r'} \right) - \frac{11 C_F a_s}{12 m_t c^2} \left(\frac{1}{r}\frac{d}{dr} r + \frac{1}{r'}\frac{d}{dr'} r' \right) \right] G(r,r') + \frac{1}{4 m_t c^2}\, \frac{1}{4\pi r r'}\, \delta(r - r'), \tag{B8}$$

where $G(r,r')$ is defined from a simplified Hamiltonian in Eq. (4). Using standard perturbative expansion in quantum mechanics, one can show that both sides of (B8) coincide up to (and including) $O(1/c^2)$ in the series expansion in $1/c$, and that also in the vicinity of each resonance pole, the pole position and the residue coincide up to the same order. One may then express the Fourier transform of (B8) in terms of the momentum-space Green functions defined in Eqs. (21)–(23). In addition, in the limit $r_0 \to 0$ one can justify a replacement

$$\frac{d}{dr_0} r_0 \tilde{G}(p;r_0) \to \left(1 - \frac{1}{2} C_F m_t a_s r_0\right) \tilde{G}(p;r_0). \quad \text{(B9)}$$

By including the $\gamma t\bar{t}$ vertex in the Born diagram for $e^+e^- \to t\bar{t} \to bW^+\bar{b}W^-$ and integrating over the bW phase space, one obtains the momentum distribution formula (19). All r_0-dependent factors multiplying $\tilde{G}(p;r_0)$ are combined with $C(r_0)$ and included in the vertex renormalization constant given in (19).

APPENDIX C: PROOF OF UNITARITY RELATION

In order to prove the unitarity relation between Eqs. (3) and (19), it is sufficient to show

$$\begin{aligned}
\mathrm{Im}\left[\left(1 + \frac{E + i\Gamma_t}{6m_t}\right) G(r_0,r_0)\right]
&= \int \frac{d^3\mathbf{p}}{(2\pi)^3} \Gamma_t \Bigg\{ \left(1 + \frac{2E}{3m_t}\right) |\tilde{G}(p;r_0)|^2 \\
&\quad + \frac{3}{2} C_F \alpha_s(\mu)^2 \,\mathrm{Re}[\tilde{G}_{1/r}(p;r_0)\, \tilde{G}(p;r_0)^*] \\
&\quad - \frac{11}{6} C_F \alpha_s(\mu)^2 \,\mathrm{Re}[\tilde{G}_{ip_r}(p;r_0)\, \tilde{G}(p;r_0)^*] \\
&\quad + \frac{1}{6m_t} \frac{\sin(pr_0)}{pr_0} \mathrm{Re}[\tilde{G}(p;r_0)] \Bigg\}. \qquad \text{(C1)}
\end{aligned}$$

This equality follows readily from a combination of the identities

$$\begin{aligned}
&\int \frac{d^3\mathbf{p}}{(2\pi)^3} \Gamma_t \Bigg\{ \left(1 + \frac{E}{2m_t}\right) |\tilde{G}(p;r_0)|^2 \\
&\quad + \frac{3}{2} C_F \alpha_s(\mu)^2 \,\mathrm{Re}[\tilde{G}_{1/r}(p;r_0)\, \tilde{G}(p;r_0)^*] \Bigg\} \\
&\quad = \mathrm{Im}\, G(r_0,r_0), \qquad \text{(C2)}
\end{aligned}$$

$$\int \frac{d^3\mathbf{p}}{(2\pi)^3} \Gamma_t \,\mathrm{Re}[\tilde{G}_{ip_r}(p;r_0)\, \tilde{G}(p;r_0)^*] = 0, \qquad \text{(C3)}$$

$$\int \frac{d^3\mathbf{p}}{(2\pi)^3} \Gamma_t \frac{\sin(pr_0)}{pr_0} \mathrm{Re}[\tilde{G}(p;r_0)] = \mathrm{Im}[i\Gamma_t G(r_0,r_0)], \qquad \text{(C4)}$$

and neglecting terms suppressed by $O(\alpha_s^4)$.

Proof of Eq. (C2)

Let us define an operator

$$G = \left[\frac{\mathbf{p}^2}{m_t} + V(r) - \left(\omega + \frac{\omega^2}{4m_t}\right)\right]^{-1}. \qquad \text{(C5)}$$

Then

$$\begin{aligned}
\mathrm{Im}\, G &= G^\dagger \frac{(G^{-1})^\dagger - G^{-1}}{2i} G = -\, G^\dagger \mathrm{Im}[G^{-1}] G \\
&= G^\dagger \left(\Gamma_t + \frac{E\Gamma_t}{2m_t} + \frac{3C_F\alpha_s}{2m_t r}\right) G, \qquad \text{(C6)}
\end{aligned}$$

where the imaginary part of any operator X is defined as $\mathrm{Im}X = (X - X^\dagger)/(2i)$. Sandwiching both sides by $\langle r_0|$ and $|r_0\rangle$, and inserting a completeness relation on the right-hand-side, one obtains Eq. (C2).

Proof of Eq. (C3)

$$\begin{aligned}
&\int \frac{d^3\mathbf{p}}{(2\pi)^3} \Gamma_t \,\mathrm{Re}[\tilde{G}_{ip_r}(p;r_0)\, \tilde{G}(p;r_0)^*] \\
&= \int \frac{d^3\mathbf{p}}{(2\pi)^3} \frac{\Gamma_t}{\alpha_s m_t} [\langle r_0|G^\dagger|p\rangle\langle p|ip_r G|r_0\rangle \\
&\quad + \langle r_0|G^\dagger (ip_r)^\dagger|p\rangle\langle p|G|r_0\rangle] \\
&= \frac{\Gamma_t}{\alpha_s m_t} \langle r_0|G^\dagger\, ip_r\, G + G^\dagger\, (ip_r)^\dagger\, G|r_0\rangle = 0, \qquad \text{(C7)}
\end{aligned}$$

where we used hermiticity of p_r in the last line.

Proof of Eq. (C4)

$$\begin{aligned}
\mathrm{Im}[i\Gamma_t G(r_0,r_0)] &= \frac{\Gamma_t}{2} \langle r_0|G + G^\dagger|r_0\rangle \\
&= \frac{\Gamma_t}{2} \int \frac{d^3\mathbf{p}}{(2\pi)^3} [\langle r_0|G|p\rangle\langle p|r_0\rangle + \langle r_0|p\rangle \\
&\quad \times \langle p|G^\dagger|r_0\rangle] \\
&= \int \frac{d^3\mathbf{p}}{(2\pi)^3} \Gamma_t \frac{\sin(pr_0)}{pr_0} \mathrm{Re}[\tilde{G}(p;r_0)]. \qquad \text{(C8)}
\end{aligned}$$

Note that the S-wave component of $e^{i\mathbf{p}\cdot\mathbf{r}}$ is given by $\sin(pr)/(pr)$.

[1] V.S. Fadin and V.A. Khoze, Pis'ma Zh. Éksp. Teor. Fiz. **46**, 417 (1987) [JETP Lett. **46**, 525 (1987)]; Yad. Fiz. **48**, 487 (1988) [Sov. J. Nucl. Phys. **48**, 309 (1988)].
[2] V.S. Fadin and V.A. Khoze, Yad. Fiz. **53**, 1118 (1991) [Sov. J. Nucl. Phys. **53**, 692 (1991)].
[3] M. J. Strassler and M. E. Peskin, Phys. Rev. D **43**, 1500 (1991).
[4] V. S. Fadin and O. I. Yakovlev, Yad. Fiz. **53**, 1111 (1991) [Sov. J. Nucl. Phys. **53**, 688 (1991)].
[5] Y. Sumino, K. Fujii, K. Hagiwara, H. Murayama, and C.-K. Ng, Phys. Rev. D **47**, 56 (1993).
[6] M. Ježabek, J.H. Kühn, and T. Teubner, Z. Phys. C **56**, 653 (1992).
[7] M. Ježabek and T. Teubner, Z. Phys. C **59**, 669 (1993).
[8] H. Murayama and Y. Sumino, Phys. Rev. D **47**, 82 (1993).
[9] P. Igo-Kemenes, M. Martinez, R. Miquel, and S. Orteu, talk given at the Workshop on Physics and Experiments with Linear e^+e^- Colliders, Waikoloa, Hawaii, 1993.
[10] J.H. Kühn, in *Physics and Experiments with Linear e^+e^- Colliders*, edited by F.A. Harris *et al.* (World Scientific, Singapore, 1993), p.72.
[11] K. Melnikov and O. Yakovlev, Phys. Lett. B **324**, 217 (1994).
[12] Y. Sumino, Ph.D. thesis, University of Tokyo, 1993.
[13] Y. Sumino, Acta Phys. Pol. B **25**, 1837 (1994).
[14] V. S. Fadin, V. A. Khoze, and A. D. Martin, Phys. Rev. D **49**, 2247 (1994); Phys. Lett. B **320**, 141 (1994).
[15] K. Fujii, T. Matsui, and Y. Sumino, Phys. Rev. D **50**, 4341 (1994).
[16] W. Mödritsch and W. Kummer, Nucl. Phys. **B430**, 3 (1994); W. Kummer and W. Mödritsch, Z. Phys. C **66**, 225 (1995).
[17] M. Ježabek, in *Physics at LEP200 and Beyond*, edited by T. Riemann and J. Blumlein [Nucl. Phys. B (Proc. Suppl.) **37**, 197 (1994)].
[18] R. Harlander, M. Ježabek, J.H. Kühn, and T. Teubner, Phys. Lett. B **346**, 137 (1995).
[19] V. S. Fadin, V. A. Khoze, A. D. Martin, and A. Chapovskii, Phys. Rev. D **52**, 1377 (1995).
[20] W. Mödritsch, Nucl. Phys. **B475**, 507 (1996).
[21] R. Harlander, M. Ježabek, J. H. Kühn, and M. Peter, Z. Phys. C **73**, 477 (1997).
[22] M. Peter and Y. Sumino, Phys. Rev. D **57**, 6912 (1998).
[23] A. H. Hoang and T. Teubner, Phys. Rev. D **58**, 114023 (1998).
[24] K. Melnikov and A. Yelkhovsky, Nucl. Phys. **B528**, 59 (1998).
[25] O. Yakovlev, Phys. Lett. B **457**, 170 (1999).
[26] M. Ježabek, J.H. Kühn, M. Peter, Y. Sumino, and T. Teubner, Phys. Rev. D **58**, 014006 (1998).
[27] O. Yakovlev and A. Yelkhovsky, Phys. Lett. B **438**, 341 (1998).
[28] M. Beneke, A. Signer, and V. A. Smirnov, Phys. Lett. B **454**, 137 (1999).
[29] J. H. Kühn and T. Teubner, Eur. Phys. J. C **9**, 221 (1999).
[30] A. H. Hoang, M. C. Smith, T. Stelzer, and S. Willenbrock, Phys. Rev. D **59**, 114014 (1999).
[31] M. Beneke, Phys. Lett. B **434**, 115 (1998).
[32] K. Melnikov (private communication).
[33] N. Gray, D. J. Broadhurst, W. Grafe, and K. Schilcher, Z. Phys. C **48**, 673 (1990).
[34] M. Ježabek and J.H. Kühn, Nucl. Phys. **B314**, 1 (1989).
[35] M. Ježabek and J.H. Kühn, Phys. Rev. D **48**, R1910 (1993); **49**, 4970(E) (1994).
[36] C. R. Schmidt, Phys. Rev. D **54**, 3250 (1996).
[37] G. Siopsis, hep-ph/9807556.
[38] W. Beenakker, F. A. Berends, and A. P. Chapovsky, Phys. Lett. B **454**, 129 (1999).
[39] M. Ježabek, M. Peter, and Y. Sumino, Phys. Lett. B **428**, 352 (1998).
[40] W. Fischler, Nucl. Phys. **B129**, 157 (1977).
[41] A. Billoire, Phys. Lett. **92B**, 343 (1980).
[42] M. Peter, Phys. Rev. Lett. **78**, 602 (1997); Nucl. Phys. **B501**, 471 (1997).
[43] Y. Schröder, Phys. Lett. B **447**, 321 (1999).
[44] B. Grinstein and I. Z. Rothstein, Phys. Rev. D **57**, 78 (1998).
[45] A. Czarnecki and K. Melnikov, Phys. Rev. Lett. **80**, 2531 (1998).